Mon. Not. R. Astron. Soc. **000**, 000–000 (0000) Printed 5 February 2008 (MN LaTeX style file v1.4)

Near-Infrared Fundamental Plane of Elliptical Galaxies

B. Mobasher[1], R. Guzmán[2], A. Aragón-Salamanca[3], S. Zepf[4]
[1] *Astrophysics Group, Blackett Laboratory, Imperial College, Prince Consort Rd, London SW7 2BZ, UK*
[2] *UCO/Lick Observatory, University of California, Santa Cruz, 1156 High Street, Santa Cruz, CA 95064, USA*
[3] *Institute of Astronomy, Madingley Road, Cambridge CB3 0HA, UK*
[4] *Department of Astronomy, University of California, Berkeley, CA 94720, USA*

5 February 2008

ABSTRACT

Near-infrared (2.2 μm) observations of a sample of 48 elliptical galaxies in the Coma cluster have been carried out and used to study the near-ir fundamental plane (FP) of ellipticals in this cluster. An rms scatter of 0.072 dex was found for this relation, similar to that of its optical counterpart, using the same sample of galaxies. This corresponds to an uncertainty of 18% in distances to individual galaxies derived from this relation. The sensitivity of the near-infrared FP to the star formation or changes in metallicity and stellar population among the ellipticals was explored and found to be small. Although, a likely source of scatter in this relation is contributions from the Asymptotic Giant Branch (AGB) population to their near-infrared light. Allowing for observational uncertainties, we find an intrinsic scatter of 0.060 dex in the near-ir FP. The cluster galaxies presented here, provide the zero-point for the peculiar velocity studies, using the near-infrared FP.

Changes in the slopes of the $D-\sigma$ and $L-\sigma$ relations of ellipticals between the optical and near-infrared wavelengths were investigated and found to be due to variations in metallicity or age (or a combination of them). However, it was not possible to disentangle the effects of age and metallicity in these relations.

We find $M/L \propto M^{\alpha}$ with $\alpha = 0.18 \pm 0.01$ at the near-ir and $\alpha = 0.23 \pm 0.01$ at the optical wavelengths, using the same sample of galaxies. This relation is interpreted as due to a mass-metallicity effect or changes in age or the IMF slope with mass. Using evolutionary population synthesis models, we find that the effects of age and metallicity decouple on the $(M/L)_K$ vs. Mg_2 and $(M/L)_K$ vs. (V−K) diagrams. The models suggest that the observed trends on these relations may be due to an age sequence while metallicity mainly contributing to the scatter.

Key words: Galaxies: elliptical– Galaxies: photometry– Galaxies: fundamental parameters– Galaxies: stellar content– Galaxies: structure– Galaxies: evolution– Galaxies:clusters:individual:Coma– infrared:Galaxies

1 INTRODUCTION

Elliptical galaxies define a Fundamental Plane (FP) on the 3-parameter space of the half-light radius R_e, the mean surface brightness within that radius $\langle SB \rangle_e$, and the central velocity dispersion σ (Djorgovski & Davis 1987; Dressler et al. 1987a). The scatter around the FP is only ~ 0.08 dex in $\log R_e$ for cluster ellipticals. The existence of this scaling relation provides one of the most important constraints to model the formation and evolution of elliptical galaxies (Bender et al 1993; Guzmán et al. 1993; Renzini & Ciotti 1993; Zepf & Silk 1996). Also, it can be used as a distance indicator to trace the non-Hubble motions in the local universe (Dressler et al 1987b; Lucey & Carter 1988; Lynden-Bell et al. 1988), and potentially as a cosmological evolutionary probe when studying the FP for cluster ellipticals at higher redshifts (Franx et al. 1996; van Dokkum & Franx 1996; Barger et al. 1996).

The biparametric nature of elliptical galaxies suggests that the virial theorem is the main constraint on their structure (Faber et al. 1987; Djorgovski 1987; but see Guzmán et al. 1993). The tilt of the FP relative to the virial equation implies a systematic variation either in the IMF, the shape of the light profile, the age and metallicity or the dark and luminous matter distribution with galaxy mass (Guzmán et al. 1993; Ciotti et al. 1996). Our understanding of the physical mechanisms responsible for such variation is still at a very early stage. Moreover, substantial fine-tuning is required to

produce the tilt while preserving the small scatter of the galaxy distribution along the FP (Ciotti et al. 1996). The tightness of the FP for cluster ellipticals is clear evidence for a very standardized and synchronized production of ellipticals, with the vast majority of their stellar populations being formed at redshifts $z > 2$, at least for those ellipticals in clusters (Renzini 1995; Ellis et al. 1996). However, there is growing evidence that ellipticals outside the core of rich clusters tend to have a younger stellar component (Rose 1985; Pickles 1985; Bower et al. 1990). As a result, non-cluster ellipticals at a given R_e and/or σ have, on average, bluer colours, higher effective surface brightnesses, and lower Mg_2 line strength indices as compared to their cluster counterparts (Larson et al. 1980; Guzmán et al. 1992; de Carvalho & Djorgovski 1992). This systematic variation of stellar population properties due to the environment may in turn translate into a zero-point offset of the FP-based distance indicators (such as $D_n - \sigma$) and thus lead to spurious peculiar velocities (Kaiser 1988; Silk 1989; de Carvalho & Djorgovski 1992; but see Burstein et al. 1990). Indeed, using stellar population evolutionary models, Guzmán & Lucey (1993) have combined the FP with the $\sigma - Mg_2$ relation to create a new distance indicator that is independent of age/environmental differences. When the new distance indicator is applied to the ellipticals with a younger stellar component, the large positive peculiar motions previously reported are greatly removed (Guzmán & Lucey 1993).

Most studies on the FP have been done at optical wavelengths. Observations in the infrared may shed light on the origin of the tilt and scatter of the FP by probing a wavelength region with a different sensitivity to stellar population effects. In particular, the effect of age and/or metallicity variations in ellipticals is expected to be greatly reduced in the K-band (i.e., $2.2\mu m$) since the galaxy light at these wavelengths is mainly sensitive to the old stellar component and is less affected by line-blanketing. Moreover, the K-band is significantly less sensitive to both the presence of dust in ellipticals and galactic extinction. The new K-band FP can also be used as an independent distance indicator to check for stellar-population effects on the peculiar velocity measurements derived using the FP in the optical. Early work on the infrared FP relied on single element photometry and hence, lacked detailed surface photometry (Gregg 1995a; Recillas-Cruz et al. 1990, 1991). Recently, Pahre et al. (1996) have shown that the coefficients and scatter of the FP in the K-band for a sample of ellipticals in five nearby clusters are similar to those derived in the optical. They conclude that the observed small differences are consistent with the reduction of metallicity effects in the near-infared bandpass.

In this paper, we present the first results of a large-scale K-band survey of elliptical galaxies located in different environments (i.e., clusters, field and Great Attractor region). Here we study the coefficients and scatter of the K-band FP, using accurate surface photometry for a homogeneous sample of 48 galaxies in the Coma cluster. By considering a single cluster, we avoid introducing artificial scatter due to distance errors or non-universality of the FP. The aim of this study is three fold: 1) to shed light on the origin of the FP by using a wavelength region with a different sensitivity to the stellar population effects than the optical; 2) to establish the intrinsic scatter on the K-band FP; and 3) to set the zero-point of the new infrared distance scale using the K-band FP for Coma cluster ellipticals.

In the next section, the observations and data reduction are discussed. This is followed by the study of the near-infrared scaling laws in section 3. The implications for the origin of the FP and the new distance scale are discussed in section 4. Finally, our conclusions are summarized in section 5.

2 OBSERVATIONS AND DATA REDUCTION

2.1 Observations

The observations used in this study were made at the United Kingdom Infrared Telescope (UKIRT) in the period 28-30th April 1994. Near-infrared K-band (2.2 μm) images of 48 elliptical galaxies in the Coma cluster were obtained, using the 256×256 infrared array detector (IRCAM3) with a pixel size of $0.286''$. The galaxies are selected to be ellipticals (i.e. no lenticulars) from the sample in Lucey et al (1991, Table 6) with reliable velocity dispersion and optical photometry. They are located at different distances from the center of the Coma cluster ($\alpha = 12\ 57\ 19$ $\delta = 28\ 15\ 51$ (1950)). Also, they have optical half-light diameters smaller than $1'$, fitting the field of view of the IRCAM3. An exposure time of 10 sec. was used with 6 co-adds. For each object, nine exposures were taken at different positions, separated by $20''$, giving a total integration time of 9 mins. per object. This technique was employed to avoid the effect of bad pixels and cosmic rays, to construct reliable flatfields for each frame and to measure the sky background. Surface photometry of smaller galaxies can be affected by the seeing condition which was estimated to be around $1''$. The sensitivity of the results to this effect will be explored in the following analysis. Observations of faint UKIRT standards were also carried out during the night and were used to monitor the accuracy of the photometry.

2.2 Data Reductions.

Observations were dark subtracted using the dark frames closest (in time) to each object. For each galaxy, the nine mosaic frames were then median filtered and the result normalised to its median pixel value to construct the flatfield. The dark subtracted, flatfielded frames were then registered and mosaiced to increase the S/N. The data reduction was carried out, using the CCDPACK software in the STARLINK environment. The median sky value was then estimated for each frame individually and used to sky-subtract that frame. The mosaic frames, providing a larger sky coverage than single frames, were used for this purpose and the sky values were measured as far away from the center of galaxy as possible. The variations in sky estimates at different positions on the frame were monitored, giving a measure of the uncertainties in these values. This did not exceed 0.02 mag., even for the bigger galaxies for which the uncertainties are larger. Therefore, this is taken as our estimated error due to sky subtraction.

The standard stars were reduced in the same way and used to establish the extinction relation for each night.

Changes in the zero-points, estimated from the standards throughout the run (internal photometric error), is 0.02 mag.

2.3 Photometry

Aperture photometry was performed on the final images and used to construct the near-ir growth curves for individual galaxies. The magnitudes were corrected for atmospheric extinction, Galactic absorption (taking $A_K = 0.085A_B$ (Pahre et al. 1996) and the median A_B for the Coma galaxies from Faber et al (1989)) and redshift effect (assuming $k(z) = 3.3z$ for ellipticals at the K-band (Persson et al (1979)). The photometric accuracy is checked by comparing magnitudes of the objects in our sample with the same galaxies from other independent observations. The K-band magnitudes for 18 galaxies in the present sample, in common with Bower et al (1992), are measured over an aperture of 17″ diameter, used by these authors. The two magnitudes are compared in Figure 1a and show a mean offset of

$$\langle K_{this\ study} - K_{Bower\ et\ al.} \rangle = -0.06 \pm 0.01$$

with an rms scatter of 0.03 mag. Assuming equal errors in both the data sets, this corresponds to an internal error of $0.03/\sqrt{2} = 0.02$ mag. per galaxy, consistent with that claimed by Bower et al (1992). The cause of the zero-point offset between the two data sets is not clear but is likely to be due to different detectors used. However, since the data here are 2-D and Bower et al's is based on single element photometry, we expect to have a more accurate control over the sky subtraction in our data. Neverthless, the offset is relatively small.

The growth curves, corrected for Galactic absorption and redshift effects, were used to construct near-infrared surface brightness profiles for each galaxy, corrected for the $(1+z)^{-4}$ surface brightness dimming. Near-infrared isophotal diameters, corresponding to a mean surface brightness of 16.5 mag/arcsec^2 are then estimated. This isophote was adopted to be directly comparable with the mean optical surface brightness of 19.8 mag/arcsec.^{2} (assuming $V - K = 3.3$ mag. for ellipticals) used in the optical $D_V - \sigma$ relation. To examine the accuracy of our surface photometry, we have also obtained data for a sub-set of 12 ellipticals in our sample, using the IRIS at the Anglo-Australian Telescope (March 1995). These diameters, measured at a mean K-band surface brightness of 16.5 mag./arcsec^2, are compared with the present measurements in Figure 1b and show a mean offset of

$$\langle log(D_K^{UKIRT}/D_K^{AAT}) \rangle = 0.013\ dex \pm 0.006 dex$$

with an rms scatter of 0.019 dex. Assuming that the uncertainty in these measurements is shared equally between both the data sets, we estimate an observational error of 0.01 dex in $\log(D_K)$ values.

The diameters of smaller galaxies in our sample might be affected by the seeing condition. To estimate this effect, we used the models in Lucey et al (1991) and estimated the effect of 1 arcsec seeing on the aperture photometry (the observations here were done in 0.8-1.2 arcsec seeing conditions). The correction was then applied to one of our smaller galaxies and its photometric parameters were recalculated. We find that at 1 arcsec seeing conditions, an increase in $\log(D_K)$ of only 0.01 dex was needed due to seeing. The diameters of larger galaxies were almost insensitive to this effect. The range in surface brightness values between 16 and 17 mag/arcsec^2 was explored in 0.1 intervals. The results in the following sections were found to be insensitive to the actual choice of the isophote.

The near-infrared effective diameter and surface brightness (i.e. the diameter containing half the total luminosity of a galaxy and the mean surface brightness within that diameter) were calculated for galaxies in the present sample by fitting the observed K-band curve of growths to the de Vaucouleurs $r^{1/4}$ law. The accuracy of this fitting procedure was estimated by generating simulated profiles following the $r^{1/4}$ law with known effective parameters and artificially added noise, analogous to the photometric errors. An $r^{1/4}$ fit to these profiles recovers both the input effective parameters, giving errors of 0.02 *dex* and 0.03 mag/arcsec^2 in the effective diameter and surface brightness values respectively. The total K-band magnitudes are then estimated by extrapolating the $r^{1/4}$–law fit for individual galaxies to large radii, using their corresponding values of the effective diameter and surface brightness. These magnitudes are corrected for Galactic absorption and redshift, using the relations discussed above. Also, the effective surface brightness estimates are corrected for the $(1 + z)^{-4}$ dimming effect.

Finally, the K-band magnitudes, measured over an aperture of 20 arcsec. diameter are estimated and combined with their corresponding V-band data from literature, measured over the same aperture (Lucey et al 1991). The $V - K$ colours were then estimated and corrected for Galactic extinction and redshift, using the above prescription for the near-ir and the relations from Faber et al (1989) for the optical data.

2.4 The Catalogue

The sample of 48 elliptical galaxies in the Coma cluster, observed in this study, is presented in Table 1. Column 2 gives the distance (in degrees) of galaxies from the center of the cluster. In columns 3 and 4, the near-infrared (K-band) isophotal diameters in arcsec. (corresponding to a mean surface brightness of $\langle SB_K \rangle = 16.5$ mag/arcsec^2) and total magnitudes of ellipticals are presented. These are corrected for redshift effect, surface brightness dimming and Galactic absorption. Column 5 gives the optical V-band diameters (in arcsec.), corresponding to a mean surface brightness of $\langle SB_V \rangle = 19.8$ mag/arcsec^2, taken from Lucey et al. (1991). The velocity dispersion of ellipticals (log(σ)- in Km/sec), listed in column 6, are taken from Lucey et al. (1997). For galaxies with no available velocity dispersion measurements from this source, the values in Lucey et al. (1991) were converted to the above system using the common galaxies between the two samples. The velocity dispersions have an associated error of 0.03 *dex*. Columns 7 and 8 present the near-infrared effective diameters (in arcsec.) and effective mean surface brightnesses. This is followed in columns 9 and 10 by the K-band aperture magnitudes and V−K colours respectively, measured over an aperture of 20 arcsec. diameter and corrected for Galactic extinction and redshift. The Mg_2 line strengths are listed in column 11. These are also taken from Lucey et al. (1997). For galaxies with no such measurements from this reference, The Mg_2 indices from Lucey et al. (1991) are used after conversion to this system.

Table 1. The near-infrared catalogue for elliptical galaxies in Coma

	r	$\log(D_K)$	K_{tot}	$\log(D_V)$	$\log(\sigma)$	$\log(A_e)$	$\langle SB_K\rangle_e$	K_{20}	V−K	Mg_2
RB45	0.040	0.810	11.91	0.858	2.133	0.859	16.69	12.31	3.10	0.280
N4886	0.050	0.964	10.86	1.030	2.209	1.180	17.25	11.54	2.95	0.254
RB43	0.056	0.799	12.19	0.866	2.230	0.694	16.15	12.52	3.01	0.262
N4889	0.060	1.473	8.20	1.480	2.595	1.759	17.49	9.76	3.32	0.348
N4874	0.060	1.266	8.55	1.294	2.398	1.934	18.71	10.44	3.26	0.323
N4876	0.062	0.989	10.89	1.027	2.267	1.157	17.17	11.49	3.19	0.242
IC4011	0.064	0.811	11.78	0.872	2.061	0.927	16.90	12.21	3.04	0.279
N4872	0.069	1.034	11.30	1.048	2.329	0.671	15.15	11.49	3.09	0.300
RB18	0.099	0.576	12.65	0.682	2.019	0.848	17.38	13.09	2.94	0.231
IC4021	0.112	0.944	11.58	0.943	2.205	0.711	15.62	11.85	3.23	0.299
N4869	0.119	1.127	10.27	1.137	2.303	1.207	16.80	11.01	3.23	0.315
IC4012	0.125	1.003	11.40	1.000	2.258	0.681	15.30	11.67	3.30	0.292
N4867	0.135	1.043	11.12	1.050	2.352	0.796	15.59	11.47	3.17	0.307
N4864	0.144	1.157	10.15	1.126	2.289	1.290	17.09	10.91		0.286
RB155	0.161	0.770	11.95	0.820	2.083	0.910	16.98	12.39	3.11	0.264
N4906	0.181	0.997	10.89	1.033	2.228	1.100	16.88	11.47	3.17	0.288
RB257	0.209	0.828	12.16	0.864	2.200	0.609	15.70	12.47	3.09	0.279
RB167	0.212	0.858	11.51	0.897	2.174	1.013	17.06	12.05	3.16	0.266
IC4051	0.234	1.107	9.95	1.087	2.359	1.448	17.68	10.99	3.27	0.333
D204	0.404	0.792	11.84	0.861	2.114	0.942	17.04	12.30	3.05	0.268
D160-100	0.441	0.945	11.47	0.959	2.269	0.786	15.89	11.82	3.20	0.285
n4927	0.464	1.200	10.16	1.135	2.450	1.092	16.11	10.74	3.50	0.354
TT41	0.470	0.725	12.08	0.790	2.009	0.919	17.16	12.51	3.02	0.260
D160-49A	0.501	0.914	11.67	0.961	2.237	0.742	15.87	12.00	3.03	0.270
N4926	0.565	1.266	9.80	1.268	2.420	1.172	16.15	10.48	3.32	0.324
N4840	0.625	1.169	10.42	1.166	2.382	0.983	15.83	10.87	3.28	0.319
D238	0.686	0.804	12.22	0.864	2.038	0.628	15.85	12.48	2.97	0.236
N4839	0.719	1.262	9.14	1.277	2.438	1.619	17.73	10.46	3.27	0.313
N4841A	0.723	1.270	9.53	1.294	2.414	1.372	16.88	10.44	3.24	0.320
D140	0.745	0.910	11.42	0.936	2.232	0.919	16.51	11.90	3.13	0.297
D160-27	0.768	0.944	11.30	0.973	2.235	0.924	16.41	11.71	3.14	0.282
D160-37	0.782	1.064	10.88	1.068	2.359	0.912	15.94	11.31	3.26	0.301
D160-23	0.811	1.003	11.21	1.011	2.250	0.865	16.03	11.58	3.22	0.310
N4816	0.839	1.159	9.95	1.170	2.330	1.303	16.96	10.83	3.24	0.310
N4824	0.846	0.912	11.54	0.929	2.205	0.830	16.18	11.83	3.23	0.278
IC4133	0.879	0.990	11.18	1.016	2.233	0.874	16.04	11.61	3.14	0.289
N4827	1.053	1.226	9.96	1.236	2.427	1.160	16.24	10.63	3.26	0.333
N4807	1.067	1.182	10.28	1.209	2.310	1.028	15.91	10.81	3.17	0.285
IC3900	1.171	1.147	10.51	1.152	2.428	0.957	15.78	10.99	3.23	0.320
IC843	1.221	1.238	10.02	1.170	2.389	1.100	16.01	10.61	3.51	0.303
N4789	1.525	1.341	9.30	1.365	2.416	1.349	16.53	10.20	3.25	0.304
N4971	1.656	1.080	10.57	1.072	2.250	1.096	16.54	11.21	3.28	0.291
D159-89	1.986	1.023	10.70	1.075	2.232	1.159	16.98	11.37	3.10	0.273
D159-83	2.500	1.182	10.23	1.152	2.306	1.088	16.16	10.82	3.38	0.275
D160-159	2.790	1.062	10.66	1.073	2.358	1.089	16.60	11.22	3.24	0.280
N4673	3.294	1.329	9.68	1.356	2.345	1.069	15.51	10.25	3.18	0.270
D159-43	4.545	1.122	10.60	1.118	2.399	0.968	15.93	11.07	3.33	0.338
D159-41	4.750	1.012	11.11	1.025	2.277	0.876	15.98	11.51	3.23	0.324

3 THE NEAR-INFRARED SCALING LAWS

3.1 The Near-Infrared Fundamental Plane

The near-infrared fundamental plane of ellipticals in the Coma cluster is established by fitting a plane to the distribution of galaxies on the effective diameter (A_e), effective mean surface brightness ($\langle SB_K\rangle_e$) and velocity dispersion (σ) space, using the data from Table 1. A simultaneous 3-parameter fit, using 48 galaxies, gives

$$log(A_e) = (1.38 \pm 0.26) log(\sigma) + (0.30 \pm 0.02)\langle SB_K\rangle_e + c_1$$

with an rms scatter of 0.072 dex in $log(A_e)$. An edge-on view of the near-ir FP is shown in Figure 2. The shape of the near-infrared FP and its scatter is in good agreement with that found by Pahre et al (1996), using 12 ellipticals in the Coma cluster. The presence of curvature on the infrared FP is explored by investigating the dependence of the scatter in Figure 2 on the FP parameters. No relation has been found between the residuals around the FP (Δ (FP) $= 1.38\ log(\sigma) + 0.30\langle SB_K\rangle_e + c_1 - log(A_e)$) and the effective diameter or surface brightness. The observed rms scatter in the near-infrared FP corresponds to an uncertainty of 18% in distances to individual galaxies from this relation.

To investigate differences between the infrared and optical FPs, we have also constructed the optical (V-band) FP, using the same sample of 48 ellipticals listed in Table 1.

The coefficients of the optical FP, estimated by performing a 3-parameter fit to these data, correspond to 1.44± 0.04 and 0.32± 0.01 for log(σ) and $\langle SB_V \rangle_e$ respectively. The rms scatter in the optical FP here is 0.074 dex, which is similar to the rms scatter of 0.08 dex (Djorgovski and Davies 1987; Jorgensen et al 1996) and 0.07 dex (de Carvalho and Djorgovski 1992) for the B-band and 0.075 dex (Lucey et al 1991) for the V-band FP, using other independent samples.

Differences between the FP coefficients from different studies, found in literature, are mainly due to the adopted fitting mathods (i.e. taking A_e or σ as the independent variables in the least-squares solutions) or sample selection, with consideration to minimise the bias in the fit. For example, it has been estimated that a least-squares fit in $log(A_e)$, produces a bias of the order of 5% for the $log(\sigma)$ coefficient, caused by observational errors (Jorgenson et al 1996). In this study, it is attempted to reduce such biases by performing a 3 parameter fit to the FP. However, adopting different fitting methods, the FP coefficients here lie in the range 1.32–1.50 ($log(\sigma)$) and 0.30–0.32 ($< SB_e >$) at the near-infrared and 1.23–1.44 ($log(\sigma)$) and 0.30–0.35 ($< SB_e >$) at the optical wavelengths. This shows the sensitivity of the FP coefficients to the adopted fitting technique, with the values in the above range, being consistent with the present study. The FP parameters found here, also agree closely with other independent estimates of the near-infrared (Pahre et al 1996) and optical (Faber et al 1987; Guzman et al 1993) FPs.

The coefficients of the near-ir and V-band FPs are similar despite different sensitivities to the stellar population and metallicity at these wavelengths. However, a smaller rms. scatter might have been expected in the near-ir FP since at this wavelength, the light samples a more uniform stellar population and is less affected by differences in line blanketing among the ellipticals. These will be addressed later in this section.

Studies of the optical FP have revealed the presence of a young stellar population in ellipticals to be partly responsible for the observed scatter in this relation (Gregg 1995b). Moreover, at a given σ, Coma ellipticals with lower Mg_2 values have, on average, slightly larger D_V diameters, with most of them located outside the core of the cluster (i.e. r>1 deg.), indicating contributions from an intermediate age stellar population, preferentially in ellipticals in low density environments (Guzmán et al 1992). This confirms that Mg_2 features are sensitive to both the 'young' stellar population and local environment of ellipticals with the galaxies having larger contributions from the 'young' stellar populations satisfying $5.2Mg_2 - log(D_V) - 0.442 < -0.2$ (Guzmán and Lucey 1993). There are only five galaxies in our near-infrared sample which satisfy this relation (N4876, N4807,N4789, 159-83 and N4673) with four of them located at the outskirts of the cluster (r> 1 deg.). These galaxies are indistinguishable from the rest of the ellipticals on the near-ir FP in the Coma cluster (Fig 2).

The sensitivity of the near-ir FP to changes in the stellar population and metallicity among the ellipticals are further investigated by comparing the Δ (FP) values with the Mg_2 index and V-K colour residuals (at a given σ) from the $Mg_2 - \sigma$ and (V-K)$-\sigma$ relations respectively (Figure 3). No relation has been found. A similar study of the residuals diagram, using the optical FP consisting of both field and cluster ellipticals, shows a significant trend which is mainly interpreted as a stellar population effect (Prugniel and Simien 1996). However, using the sample of cluster ellipticals in this study, we find no relation between the residuals from the V-band FP and Δ (Mg_2) or Δ (V$-$K) estimates. This result has been confirmed independently by Jorgensen et al. (1996), using a different sample of elliptical galaxies in clusters. Therefore, it is not clear if the lack of correlation on the residuals diagrams in Figures 3a and 3b, using the near-infrared FP in the Coma cluster, is due to the uniformity of our cluster galaxies or, represents a genuine effect, implying that the observed scatter on this relation is not affected by metallicity or contributions from the young stellar population. These scenarios are currently explored by extending the study of the near-infrared FP to the field ellipticals.

However, it is likely that changes in contributions from the intermediate age Asymptotic Giant Branch (AGB) stars to the near-infrared light of ellipticals is partly responsible for the observed scatter in this relation. Spectroscopic observations of near-ir CO (2.3 μm) absorption features of ellipticals in clusters have revealed these objects to have a smaller population of AGB stars than those in general field (Mobasher and James 1996). Therefore, it may be possible to introduce near-ir CO features as an extra parameter to reduce the scatter on the infrared FP in the same way the Mg_2 indices were introduced to the optical FP to correct the relation for contributions from the young population (Guzmán and Lucey 1993).

Considering the measurement errors of 0.02 dex in log(A_e), 0.03 dex in log(σ), 0.03 mag/arcsec^2. in the $\langle SB_K \rangle_e$ and 0.02 mag. due to sky subtraction, and considering the fact that the errors in log(A_e) and $\langle SB_K \rangle_e$ are not independent (Kormendy 1977), we estimate an observational error of 0.040 dex for the near-ir FP. Compared with a total rms error of 0.072 dex, this gives an intrinsic scatter of 0.060 dex in the near-ir FP.

3.2 The $D_K - \sigma$ Relation

The $D_K - \sigma$ relation for our sample of 48 ellipticals in the Coma cluster is shown in Figure 4. Taking σ as the independent variable (Lynden-Bell et al. 1988), a least squares fit to the $D_K - \sigma$ relation, using all the 48 galaxies, gives

$$log(D_K) = (1.37 \pm 0.08)log(\sigma) - (2.09 \pm 0.16)$$

with an rms scatter of 0.073 dex. To explore the wavelength dependence of this relation, the optical $D_V - \sigma$ relation, using the same sample of 48 ellipticals from Table 1, is constructed. This is consistent with a slope of 1.15 ± 0.09 and rms scatter of 0.077 dex, in agreement with studies based on other independent samples (Jorgensen et al 1996; Lucey et al 1991; Djorgovski and Davies 1987).

The similarity in the rms scatter between the two relations implies that dynamical parameters or the presence of an intermediate-age stellar population contributing to the near-ir light of ellipticals are responsible for the observed scatter in the $D_K - \sigma$ relation.

The slight wavelength dependence of the slope of the isophotal diameter-velocity dispersion relation ($\sim 2\sigma$ effect) leads to a correlation between $log(D_V/D_K)$ and $log(\sigma)$–

(Figure 5) as

$$log(D_V/D_K) = (-0.18 \pm 0.03)log(\sigma) + (0.42 \pm 0.05)$$

This implies that over the range of velocity dispersions covered in our sample ($\Delta(log\sigma) \sim 0.6$), the diameters change by 10% (ie. more massive galaxies have correspondingly larger near-infrared diameters). Using the stellar synthesis models of Worthey (1994), the slope of the $\log(D_V/D_K)-\log(\sigma)$ relation, due to changes in metallicity and age, is predicted and compared with the observed relation in Fig 5. The models correspond to a range in age from 5 to 17 Gyr at a constant metallicity of [Fe/H]=0.25 and variations in metallicity from -0.25 to 0.5 at a fixed age of 12 Gyr. The two models are normalised to have $\log(D_V/D_K) = -0.01$ at 12 Gyr and [Fe/H]=0.25. These normalisations are chosen to be close to the values expected for local ellipticals. The predicted relations are consistent with the observed slope, implying that changes in age (ie. stellar population), metallicity or a combination of them among the ellipticals is responsible for the wavelength dependence of the slope of their diameter-velocity dispersion relation. However, it is not possible to disentangle the effects of age and metallicity using these models.

3.3 The $L_K - \sigma$ Relation

The total near-infrared luminosities of elliptical galaxies in the Coma cluster are used from Table 1 to establish the near-ir $L_K - \sigma$ relation. The total magnitudes are employed here in order to have this relation on the same magnitude scale as the previous studies of its optical counterpart. The $L_K - \sigma$ relation is presented in Figure 6. A least squares fit, taking σ as the independent variable and using 48 ellipticals in the Coma, gives

$$K_{tot} = (-6.78 \pm 0.50)log(\sigma) + (26.28 \pm 1.14)$$

with an rms scatter of 0.50 mag. Using the aperture magnitudes (measured over an aperture of 20 arcsec. diameter-column 4 of Table 1) gives a shallower slope of -5.35 ± 0.37 and a smaller rms scatter of 0.32 mag. The optical relation, using the total V magnitudes for the same sample of ellipticals has a slope and rms scatter of -6.51 ± 0.57 and 0.49 mag. respectively. The similarity in the slope and rms scatter between the near-infrared and optical $L - \sigma$ relations implies that dynamical and structural characteristics in ellipticals are probably as important as the photometric parameters (i.e. stellar population, metallicity and age) in defining the mass–luminosity relation in these systems. This will be explored in the following discussion.

Taking the observational errors in K (0.03 mag.), $log(\sigma)$-(0.03 dex) and sky background estimate (0.02 mag.), gives an observational error of 0.19 mag. in the $L_K - \sigma$ relation. Compared with the observed scatter of 0.50 mag., an intrinsic scatter of 0.46 mag. in the $L_K - \sigma$ relation is estimated.

It is known that the colours of elliptical galaxies are correlated with their absolute magnitudes and indirectly, with their mass, in both optical (Faber 1973; Visvanathan 1983) and infrared (Persson et al 1979; Mobasher et al 1986) wavelengths. The existence of such a relation has important implications for studies of evolution of these galaxies. This colour-absolute magnitude (mass) correlation can therefore be translated into a more direct relation between the colours and velocity dispersions in ellipticals. Using the V−K colours measured over an aperture of 20 arcsec. diameter for the sample of 47 galaxies with available such data from Table 1, the $(V - K) - log(\sigma)$ relation is presented in Figure 7. A least squares fit gives

$$V - K = (0.74 \pm 0.10)log(\sigma) + (1.51 \pm 0.19)$$

with an rms scatter of 0.083 mag. in $V-K$ colours. Using the stellar synthesis models of Worthey (1994), the $(V - K) - \sigma$ relations due to changes in age and metallicity are predicted and compared with the observed relation in Figure 7. The models are calculated for a given metallicity, [Fe/H]=0.25, and a change in age from 5 to 17 Gyrs, and a range in metallicity,$-0.25 <$ [Fe/H] < 0.5, at a constant age of 12 Gyrs. The models are normalised to have [Fe/H]=0.25 and an age of 12 Gyrs at $V - K = 3.35$ mag., the values expected for local ellipticals. They are consistent with the observed $(V - K) - \sigma$ relation, again indicating that changes in either age or metallicity (or a combination of them) among the ellipticals are, at least, partly responsible for this relation. However, these models cannot disentangle the effects of age and metallicity on the $(V - K) - \sigma$ plane (Fig. 7). Recent studies also propose the presence of a mass-metallicity relation among the cluster ellipticals (Kodama & Arimoto 1996) with the metallicity being the more fundamental parameter.

To explore if the above results are model dependent, we investigate the behaviour of the observable parameters in ellipticals to changes in age and metallicity, using independent stellar synthesis models (Bruzual and Charlot 1996). At a fixed age of 12 Gyrs and over the metallicity range $-1.64 <$ [Fe/H] < 1.008, we predict a slope of $\Delta(V - K)/\Delta(Mg_2) = 5.23$ on the (V-K)–Mg_2 plane which is close to $\Delta(V - K)/\Delta(Mg_2) = 6$ found for a fixed metallicity of [Fe/H]=0.093 and a range in age from 5 to 12 Gyrs. These results are used to predict the $\Delta(V - K)/\Delta(log(\sigma))$ slope (ie. the relation in Fig. 7), using the empirical Mg_2-σ relation derived from the present sample. We find that the (V−K)-σ relations, predicted by Bruzual and Charlot (1996) model, have similar slopes due to changes in metallicity (at a given age) or age (at a given metallicity). This confirms that the results in Figures 5 and 7 are independent of the models used (ie. the metallicity and age trends are degenerate).

The $(V - K) - \sigma$ relation is independent of distance and hence, can be used to study evolution of ellipticals at different environments (i.e. in field and clusters) and redshifts. This relation can also be used to estimate velocity dispersion of ellipticals at high redshifts (for which a spectroscopic measurement of σ is difficult), using their V−K colours and allowing for evolution with redshift. The accuracy in $\log(\sigma)$ values, estimated from the (V−K)-σ relation, is 0.11 dex.

3.4 The Near-infrared M/L Ratios

The near-infrared FP found here differs, at a high confidence level, from that expected from a pure virial theorem if light directly traces the mass and if ellipticals are dynamically and structurally homologous ($D_e \propto \sigma^2 I_e^{-1}$; where I_e is the effective surface brightness in units of luminosity per area and D_e is the effective diameter). This leads

to a relation between the near-ir mass-to-luminosity ratios $log(M/L) = 2log\sigma - log(D_e/2) + 0.4\langle SB\rangle_e + a_1$ and mass $log(M) = log(D_e/2)+2log(\sigma)+a_2$ of the ellipticals (Fig. 8)-(Faber et al 1987; Djorgovski 1987). The $(M/L)_K$ and mass estimates in Figure 8 are in Solar units, assuming $z = 0.023$ for the Coma and $H_0 = 50$ km/sec/Mpc. This relation is consistent with $(M/L)_K \propto M^{\alpha}$ where $\alpha = 0.18 \pm 0.01$, in excellent agreement with $\alpha = 0.16 \pm 0.01$ estimated from a K-band study of 59 ellipticals in 5 nearby clusters (Pahre et al 1996; see also Recillas-Cruz et al 1990, 1991).

To investigate the origin of this relation and explore if it is caused by differences in the dark-to-luminous matter distribution among the ellipticals or is due to changes in metallicity, age or stellar population, we extend this study to optical wavelengths, using the same sample of galaxies (Fig. 8). The optical relation has a steeper slope of $\alpha = 0.23{\pm}0.01$, indicating that over the same range in mass, the optical and infrared M/L ratios change by factors of 3 and 2.3 respectively. The slight wavelength dependence of the slope of the M/L *vs.* M relation implies that changes in the luminous-to-dark matter distribution and/or luminosity profile among the ellipticals is not the only parameter responsible for the observed relations. Other observable parameters (see below), are also likely to be as important.

In order to have an entirely independent measurement of the slope of the M/L *vs.* M relations in the two passbands, we estimate both the M/L ratios and masses of individual galaxies, using their respective effective diameters in the near-ir and optical wavelengths. However, this introduces the unphysical effect of the dependence of the dynamical mass on the wavelength in Figure 8. Therefore, the shift in the masses of the same object between the optical and near-infrared (M/L) *vs.* M relations in Figure 8 is due to differences in the shape of the surface brightness profiles in the two bands, and to observational uncertainties in the values of the effective diameters. Nevertheless, using the effective diameters measured only in one passband to estimate the mass of galaxies, the slope of the M/L *vs.* M relations remain the same as above, indicating that the conclusions in this section do not depend on different effective diameters for individual galaxies, used to estimate the mass.

The effects of stellar population, metallicity and age on the near-infrared mass-to-luminosity ratios of the ellipticals are investigated in Fig 9, using V-K colours and Mg_2 line indices. Employing the stellar synthesis models of Worthey (1994), changes in the $(M/L)_K$ with age and metallicity are calculated for 5 Gyrs $< t <$ 17 Gyrs at constant metallicities of [Fe/H]=-0.25, 0 and 0.25 and for a range in metallicity corresponding to $-0.5 < [Fe/H] < 0.5$ at a constant age of 12 Gyrs. The models, normalised to have $log(M/L)_K = -0.5$ at 12 Gyrs and [Fe/H]=0, are compared with the data in Figs 9a and 9b.

There is only a weak dependence of the near-ir mass-to-luminosity ratio on metallicity. Furthermore, the effects of age and metallicity in ellipticals, as shown in Fig. 9, decouple when using their $(M/L)_K$ estimates (ie. the age and metallicity sequences are orthogonal). Assuming the same 'collapse factor' (the ratio of the radius covering half the total mass to the effective radius) for all the elliptical galaxies in our sample. Figures 9a and 9b suggest that the age is responsible for the observed trends on both the $(M/L)_K{-}Mg_2$ and $(M/L)_K{-}(V{-}K)$ diagrams while metallicity mainly contributes to the scatter in these relations.

4 IMPLICATIONS OF THE NEAR-INFRARED FUNDAMENTAL PLANE

The near-infrared FP is less affected by differences in line blanketing, metallicity and stellar population among the ellipticals, compared to its optical counterpart. This implies a FP relation with a potentially reduced scatter at the near-infrared wavelength. Therefore, the similarity of the rms scatter between the near-ir (0.072 dex) and optical (0.074 dex) FPs found here, was unexpected and could have important implications for constraining models of formation of ellipticals. Understanding the origin of this scatter provides a challenge in studying the evolution of elliptical galaxies.

Study of the scatter around the optical FP with ellipticity (ie. shape) has found no relation between the two quantities (Jorgensen et al 1996; Jorgensen et al 1993). As discussed in section 3.4, it is likely that changes in the $(M/L)_K$ among ellipticals is responsible for at least part of the scatter in their near-infrared FP. This may be caused by differences in age and/or metallicity (Figure 9), contributions from the Asymptotic Giant Branch (AGB) population to their near-infrared light or differences in matter distribution and the internal dynamics (ie. orbital anisotropy or rotation; Bender et al 1993) among the ellipticals. However, similarity of the scatter between the optical and near-infrared FP relations indicates that structural and dynamical differences rather than changes in age/metallicity or the AGB contributions among the ellipticals are probably responsible for the observed scatter in their near-infrared FP.

The tightness of the FP has been exploited in estimating relative distances between elliptical galaxies in the field or clusters. However, the optical FP is affected by contributions from the young population or residual star formation. Indeed, it is likely that the relatively blue ellipticals, found in the Great Attractor region, are responsible for the proposed streaming motion (Guzman and Lucey 1993). The near-infrared FP may be less sensitive to this effect (see section 3.1) and hence, the FP at this wavelength is expected to have a more stable slope and zero-point. Therefore, this relation can be used to test the reality of the streaming motion and its dependence on the non-uniformity of stellar populations among the ellipticals. For this purpose, we have performed near-ir (K-band) imaging observations of a sub-sample of ellipticals in the Great Attractor region. Using the present sample of ellipticals in the Coma cluster, we establish the zero-point of the field near-ir FP in order to use this to explore the sensitivity of the streaming motion to changes in stellar populations among the ellipticals. These results will be presented in a forthcoming paper.

Recent studies have indicated that elliptical galaxies are not the homogeneous population once assumed and are likely to have a complex evolutionary history involving interaction, starburst and infall of material (White and Frenk 1991; Cole et al. 1994). This leads to changes in the luminosity, mass and morphology of these galaxies with time, implying that their progenitors may be distinctly different from the galaxies we see today. A study of the FP of ellipticals at high redshift is needed to address these scenarios.

Recently, using the high resolution imaging capability of the Hubble Space Telescope and spectroscopic facilities on the largest ground-based telescopes (MMT and Keck), it has become possible to explore the evolution of the optical FP and M/L of ellipticals with redshift (Franx et al 1996; van Dokkum & Franx 1996; Barger et al 1996). This reveals a FP similar to those at low redshift with a comparable scatter. However, the observed change in the optical M/L is found to be smaller than that expected from population synthesis models based on a given metallicity, IMF and formation redshift (van Dokkum & Franx 1996). With the installation of the near-infrared (NICMOS) detectors on the HST, it is now possible to extend this study to longer wavelengths. The near-infrared light mainly measures the integrated star formation and hence, is more closely related to the mass function of the ellipticals. Therefore, study of the evolution of near-infrared FP and M/L of ellipticals with redshift constrains the infall and merging in these galaxies and is needed for a careful interpretation of the evolution of the luminosity function of galaxies.

5 CONCLUSIONS

The results of this study can be summarised as follows:

(i) the near-infrared (2.2 μm) fundamental plane of elliptical galaxies in the Coma cluster is studied, using a sample of 48 galaxies. This shows an rms scatter of 0.072 dex, similar to its optical counterpart, corresponding to an accuracy of 18% in distances derived from this relation.

No relation is found between the scatter around the near-infrared FP and the V−K colours or Mg_2 line strengths in ellipticals, probably implying negligible contribution to this relation due to changes in metallicity or the young population among the Coma cluster ellipticals. The AGB stars are proposed as the likely source responsible for the observed scatter in the near-ir FP. Allowing for observational uncertainties, we estimate an intrinsic scatter of 0.060 dex in this relation.

(ii) The $D_K - \sigma$ and $L_K - \sigma$ relations are studied. These have an rms scatter of 0.073 dex and 0.50 mag. respectively, compared to scatters of 0.077 dex and 0.49 mag. for their optical counterparts. The wavelength dependence of the slopes of these relations lead to correlations between (D_V/D_K) and (V-K) with the mass (σ) of ellipticals. Using stellar synthesis models, we interprete these as due to an age or metallicity (or a combination of these two) effect. However, it is not possible to disentangle the effect of age and metallicity, using these parameters.

(iii) The relation between the M/L ratio and the mass of ellipticals ($M/L \propto M^{\alpha}$) in the Coma cluster is studied. The slight difference in the slope of this relation between the infrared ($\alpha = 0.18 \pm 0.01$) and optical ($\alpha = 0.23 \pm 0.01$) wavelengths is caused by a mass-metallicity relation and not due to changes in the luminous-to-dark matter distribution among the ellipticals.

(iv) Using the stellar synthesis models, we disentangle the effects of age and metallicity on the $(M/L)_K - Mg_2$ and $(M/L)_K -$(V−K) diagrams. The trend in these relations is interpreted as an age sequence while metallicity mainly contributs to its scatter. We propose the use of $(M/L)_K$ to separate the effects of age and metallicity in elliptical galaxies.

(v) We propose to use the near-infrared FP of ellipticals in the Coma cluster to fix the zero-point of its corresponding field sample in the Great Attractor region. This is required in order to explore the effect of stellar population and metallicity on the estimates of the streaming motion of galaxies.

Acknowledgements: We acknowledge support from the PPARC (BM), the NSF through grant AST 95-29098 (RG), the Royal Society (AAS) and the Space Telescope Science Institute through a Hubble Fellowship grant HF-1055.01-93A (SZ). We are grateful to an anonymous referee for careful reading of the manuscript.

REFERENCES

Barger, A.J., Aragón-Salamanca, A., Butcher, H.R., Couch, W.J., Dressler, A., Ellis, R.S., Oemler, A., Sharples, R.M., Smail, I. 1996, in preparation
Bender, R., Bursterin, D, Faber, S. M. 1993 Ap.J,411, 153
Bower, R.G., Lucey, J.R., Ellis, R.S. 1992, MNRAS, 254, 589
Bower, R.G., Ellis, R.S., Rose, J.A., Sharples, R.M. 1990, AJ, 99, 530
Bruzual, G., Charlot, S. 1997 in preparation
Burstein, D., Faber, S.M. & Dressler, A. 1990, Ap.J. 354, 18.
Capelato, H. V., de Carvalho, R. R., Carlberg, R. G. 1995, ApJ. 451, 525
Ciotti, L., Lanzoni, B., Renzini, A. 1996, MNRAS, 282, 1
Cole, S., Aragón-Salamanca, A., Frenk, C.S., Navarro, J.F., Zepf, S. 1994, MNRAS, 271, 781
de Carvalho, R.R., Djorgovski, S. 1992, ApJL, 387, L49
Djorgovski, S., Davis, M. 1987 ApJ, 313, 59
Djorgovski, S. 1987, in Starbursts and Galaxy Evolution, Proceedings of the Moriond Astrophysics Workshop, ed. T. X. Thuan (Gif sur Yvette: Editions Frontieȓes), 549
Dressler, A. 1987, Ap.J. 317, 1.
Dressler,A., Lynden-Bell,D., Burstein,D., Davies,R.L., Faber,S.M., Terlevich,R.J., Wegner, G. 1987a ApJ, 313,42
Dressler,A., Faber,S.M., Burstein,D., Davies,R.L., Lynden-Bell,D. Terlevich,R.J., Wegner, G. 1987b ApJ, 313, L37
Ellis, R.S. et al. 1996, ApJ, in press, astro-ph/9607154
Faber, S.M. 1973 Ap.J. 179, 731
Faber,S.M., Dressler,A., Davies,R.L., Burstein,D., Lynden-Bell,D., Terlevich,R.J., Wegner, G. 1987, in Nearly Normal Galaxies, ed. S.M. Faber, (New York: Springer-Verlag), 175
Faber,S.M., Wegner, G., Burstein,D., Davies,R.L., Dressler,A., Lynden-Bell,D., Terlevich,R.J. 1989, ApJS, 69, 763
Faber,S.M., Burstein,D. 1988, in Large-Scale Motions in the Universe. A Vatican Study Week, eds. V.C. Rubin & G.V.Coyne (Princeton: Princeton University Press), 115
Franx et al. 1996 MNRAS. in press
Gregg, M. 1995a AJ. 110, 1052.
Gregg, M. 1995b ApJ. 443, 527.
Guzmán 1994 Ph.D. Thesis. University of Durham
Guzmán, R., Lucey, J.R., Carter, D., & Terlevich, R. J. 1992 MNRAS, 1992, 257, 187.
Guzmán, R., Lucey, J.R., Bower, R.G. 1993 MNRAS, 265, 731
Guzmán, R., Lucey, J.R. 1993 MNRAS, 263, L47
Jorgensen, I., Franx, M., Kjaergaard, P. 1993 Ap.J. 411, 34
Jorgensen, I., Franx, M., Kjaergaard, P. 1996 MNRAS, 280, 167.
Kaiser, N. 1988 In: Large Scale Structure and Motions in the Universe, ICTP.
Kodoma & Arimoto 1997, A& A, in press
Kormendy J. 1977 Ap.J. 218, 333
Larson, R.B., Tinsley, B.M., Caldwell, C.N. 1980 Ap.J. 237, 692
Lucey, J.R., Guzman, R., Carter, D. & Terlevich, R.J. 1991 MNRAS. 253, 584

Lucey, J.R., Guzman, R., Steel, I., & Carter, D. 1997 MNRAS. 287, 899
Lynden-Bell,D., Faber,S.M., Burstein,D., Davies,R.L., Dressler,A., Terlevich,R.J., Wegner, G. 1988 ApJ, 326, 19
Mobasher, B., Ellis, R.S. & Sharples, R.M. 1986 MNRAS 223, 11
Mobasher, B. & James, P.A. 1996 MNRAS 280, 895
Pahre, M.A., Djorgovski, S.G., de Carvalho, R.R. 1996 ApJL., 453, L17.
Persson, S.E., Frogel, J.A., Aaronson, M. 1979, ApJS, 39, 61
Pickles, A.J. 1985, Ap.J. 296, 340
Prugniel, P. & Simien, F. 1996, A & A in press
Recillas-Cruz, E., Carrasco, L., Serrano, P.G., Cruz-Gonzalez, I. 1990, A& A, 229, 64
Recillas-Cruz, E., Carrasco, L., Serrano, P.G., Cruz-Gonzalez, I. 1991, A& A, 249, 312
Renzini, A., 1995, in Gilmore G., van der Kruit, P., eds, Stellar populations. Kluwer, Dordrecht, P. 325
Renzini, A., Ciotti, L. 1993, ApJ 416, L49
Rose, J. A. 1985 A.J. 90, 1927
Silk, J. 1989, Ap.J. 345, L1
Van Dokkum, P., Franx, M. 1996 MNRAS, 281, 985.
Visvanathan, N. 1983 Ap.J. 275, 430
White, S.D.M. & Frenk, C.S. 1991 Ap.J. 379, 52
Worthey, G. 1994 ApJS, 95, 107
Zepf, S., Silk, J. 1996 ApJ 466, 114

6 FIGURE CAPTIONS

Figure 1. (a) Comparison between the K-band magnitudes of the Coma ellipticals in common with galaxies observed in Bower et al (1992). The magnitudes are measured over an aperture of 17″ diameter, used in Bower et al.

Figure 1. (b) Comparison between the K-band isophotal diameters (at 16.5 mag/arcsec.^{2}) of a sub-set of 12 ellipticals in the Coma cluster observed both at the UKIRT (IRCAM3) and the AAT (IRIS).

Figure 2). An edge-on view of the near-infrared fundamental plane for 48 ellipticals in the Coma cluster. The line is a plane fit to the data. The rms scatter in log(A$_e$) is 0.072 dex.

Figure 3. (a). Deviations from the near-infrared fundamental plane ($\Delta(FP) = 1.38\ log(\sigma) + 0.30 < SB_K >_e + c_1 - log(A_e)$) are plotted against Δ (V−K) colour residuals from the (V−K)-log(σ) relation. The lack of correlation implies that metallicity or age do not significantly contribute to the obseved scatter on the near-infrared FP of ellipticals in the Coma cluster.

Figure 3. (b). The same as Fig. 3a for the Δ (Mg_2) residuals from the Mg_2–log(σ) relation. Again, lack of correlation indicates that changes in the young population or possible environmental dependence among the ellipticals in the Coma cluster do not contribute to the scatter on their near-infrared FP.

Figure 4). The log(D_K)-log(σ) relation for 48 ellipticals in the Coma cluster. The D_K diameters are measured at 16.5 mag/arcsec.^{2} isophote.

Figure 5). The log(D_V/D_K)-log(σ) relation for ellipticals in the Coma cluster. The lines are calculated from the stellar synthesis models of worthey (1994). They correspond to changes in age (from 5 to 12 Gyrs) at a constant metallicity of [Fe/H]=0.25 (dotted line) and changes in metallicity (−0.25 < [Fe/H]< 0.5) at a constant age of 12 Gyrs (solid line). The models are transformed to the observed parameters, using the empirical log(σ)-Mg_2 and log(D_V/D_K)- (V-K) relations (from table 1), with the Mg_2 and V-K values for a given age and metallicity taken from Worthey (1994) models. The models are normalised to have log(D_V/D_K)=−0.01 at [Fe/H]=0.25 and 12 Gyr age.

Figure 6). The K_{tot}−log(σ) relation for the Coma cluster ellipticals. The total K magnitudes are used. The relation has an rms error of 0.5 mag.

Figure 7). The (V−K)−log(σ) relation for the Coma ellipticals. Colours are measured over an aperture of 20″ diameter. The lines are calculated from the stellar synthesis models of Worthey (1994). They correspond to changes in age from 5 to 17 Gyrs at a constant metallicity of [Fe/H]=0.25 (dotted line) and changes in metallicity from [Fe/H]=-0.25 to [Fe/H]=0.5 at a constant age of 12 Gyr (solid line). The model estimates for σ are calculated using the empirical relation as in Fig. 5. It is not possible to disentangle the effects of age and metallicity from this relation.

Figure 8). Correlation between the near-infrared ($\bullet$) and optical ($*$) mass-to-luminosity ratio; $log\ (M/L) = 2log\sigma - log\ (D_e/2) + 0.4\langle SB_e\rangle + a_1$ and mass; log (M) = $log(D_e/2) + 2log(\sigma) + a_2$ for the Coma ellipticals. The same sample of galaxies are used in both cases. The zero-points correspond to $a_1 = -10.67$ and -11.24 for the near-infrared and optical wavelengths respectively and $a_2 = 5.47$. Both the mass-to-luminosity ratio and mass are in solar units. For each wavelength, the mass corresponding to the effective diameter for that wavelength is plotted, leading to a slight difference in the mass estimated for the same objects in the near-infrared and optical relations.

Figure 9 (a). Changes in the near-infrared mass-to-luminosity ratios in Solar units (calculated as in Fig. 8) with the V−K colours. The lines are predictions from the stellar synthesis model of Worthey (1994) and correspond to a change in age from 5 to 17 Gyrs at a constant metallicity of [Fe/H]=-0.25 (dashed line) and [Fe/H]=0 (dotted line) and a change in metallicity from [Fe/H]=−0.5 to [Fe/H]=0.25 at a constant age of 12 Gyrs (solid line). The models are normalised to have log(M/L)$_K$=−0.50 at [Fe/H]=0 and an age of 12 Gyrs.

Figure 9 (b). The same as Fig 9a for the Mg_2 features. The lines are predictions from the stellar synthesis model of Worthey (1994) and correspond to a change in age from 5 to 17 Gyrs at a constant metallicity of [Fe/H]=0.25 (dashed line) and [Fe/H]=0 (dotted line) and a change in metallicity from [Fe/H]=−0.5 to [Fe/H]= 0.5 at a constant age of 12 Gyrs (solid line). The models are normalised to have log(M/L)$_K$=−0.50 at [Fe/H]=0 and an age of 12 Gyrs.

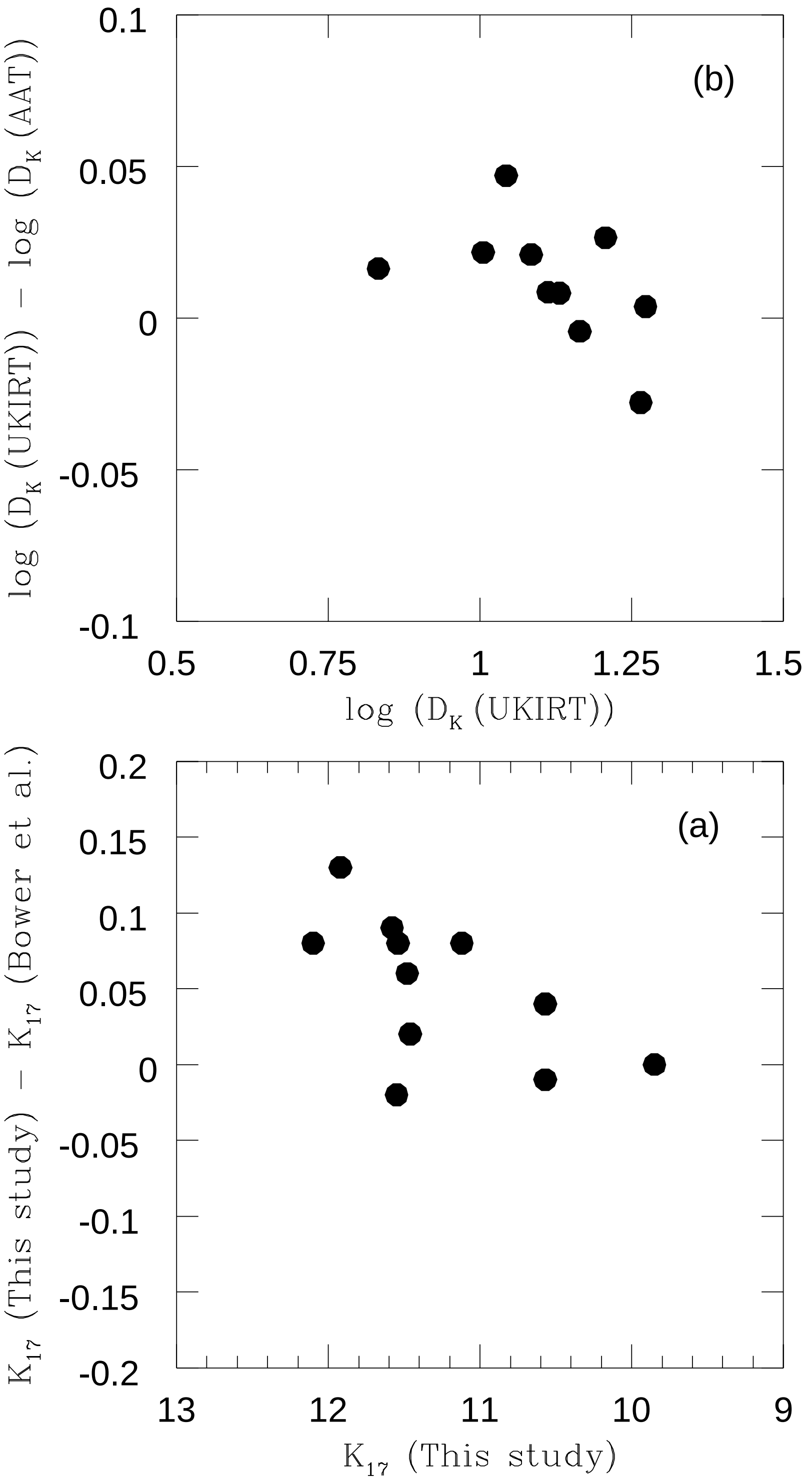

(b)
log (D$_K$ (UKIRT)) − log (D$_K$ (AAT))
log (D$_K$ (UKIRT))
0.1
0.05
0
-0.05
-0.1
0.5
0.75
1
1.25
1.5
(a)
K$_{17}$ (This study) − K$_{17}$ (Bower et al.)
K$_{17}$ (This study)
0.2
0.15
0.1
0.05
0
-0.05
-0.1
-0.15
-0.2
13
12
11
10
9

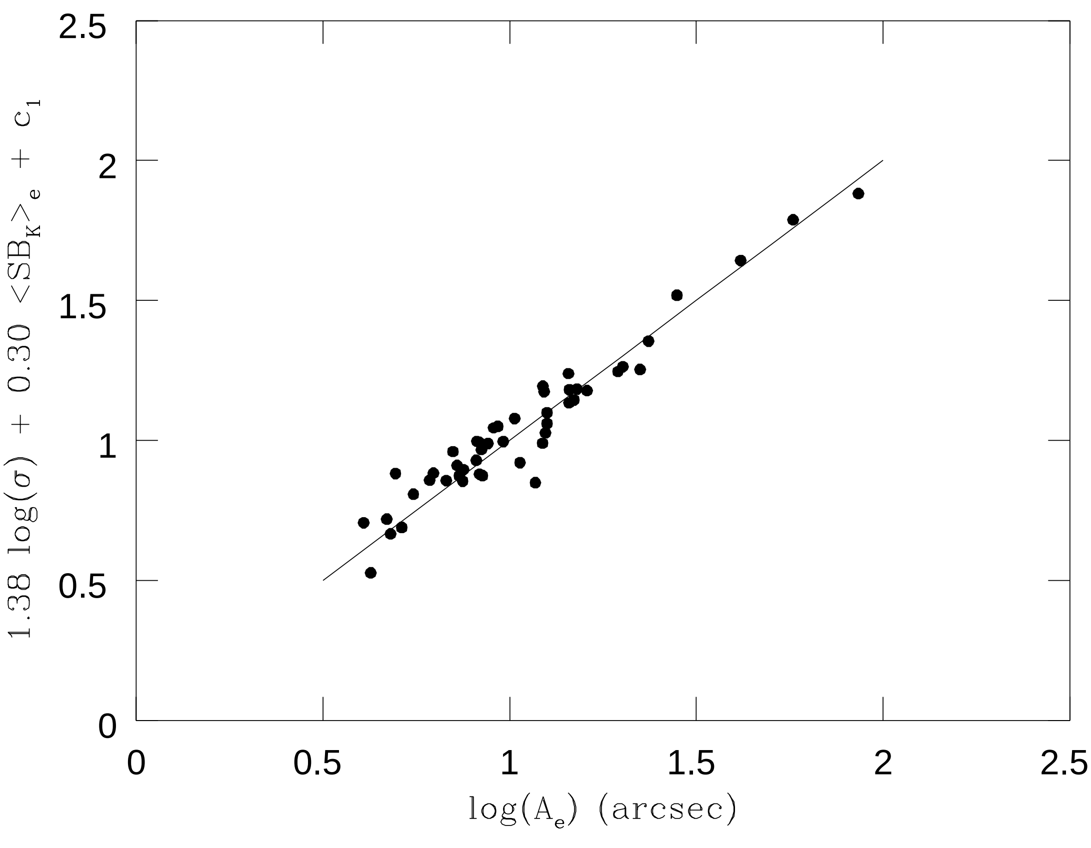

$1.38\ \log(\sigma) + 0.30\ <SB_K>_e + c_1$
$\log(A_e)$ (arcsec)

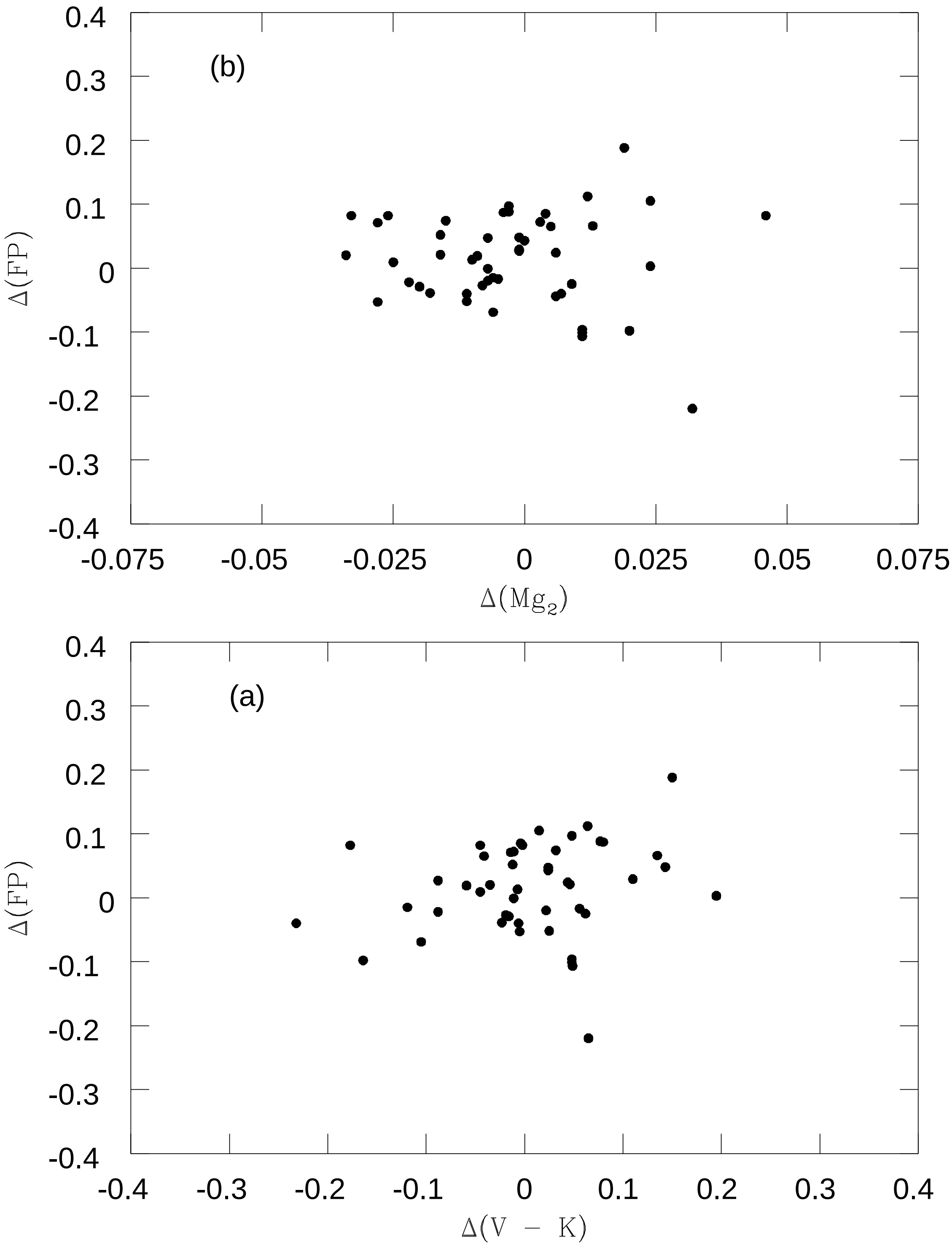

(b)
0.4
0.3
0.2
0.1
0
-0.1
-0.2
-0.3
-0.4
-0.075
-0.05
-0.025
0
0.025
0.05
0.075
Δ(FP)
Δ(Mg2)
(a)
0.4
0.3
0.2
0.1
0
-0.1
-0.2
-0.3
-0.4
-0.4
-0.3
-0.2
-0.1
0
0.1
0.2
0.3
0.4
Δ(FP)
Δ(V − K)

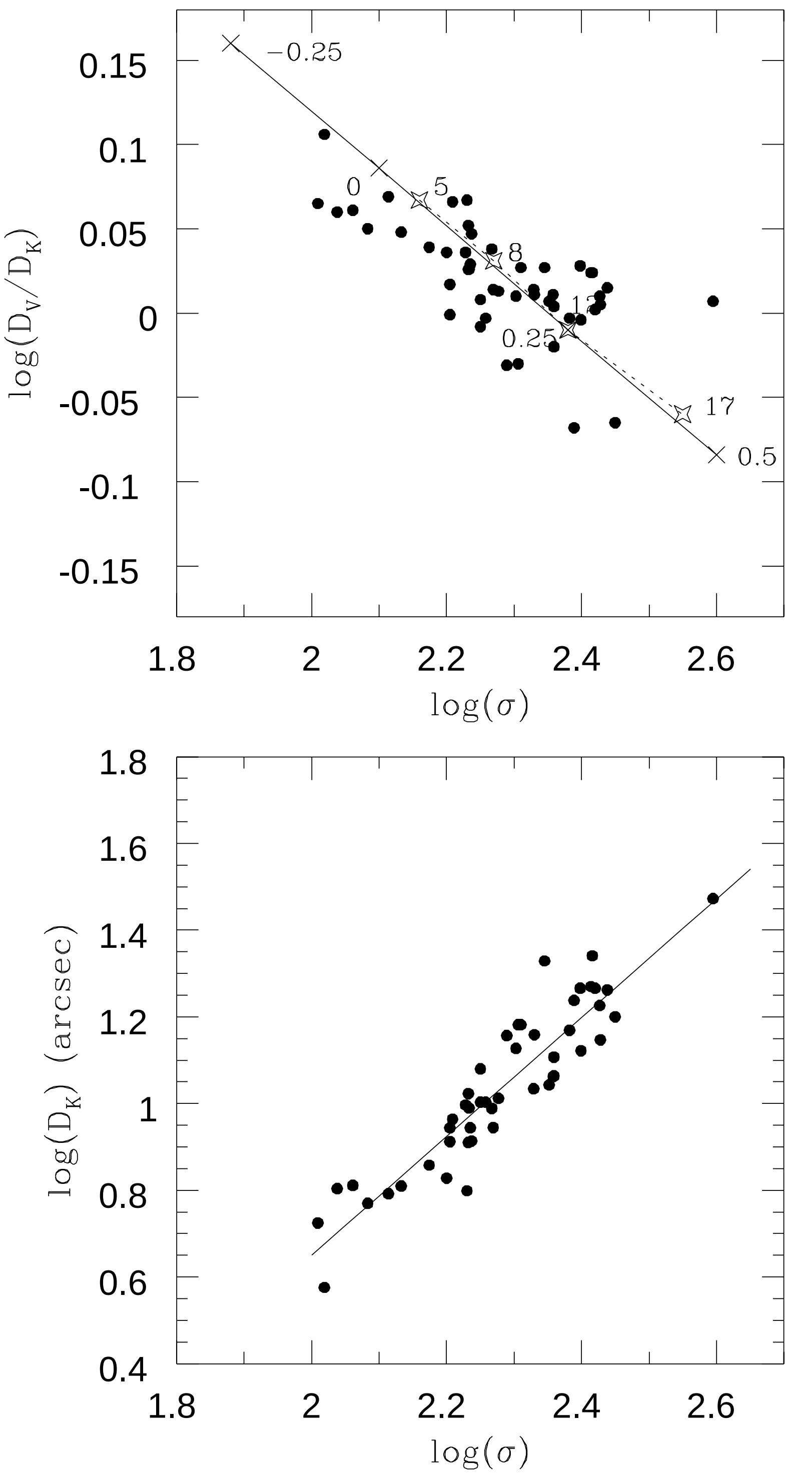

0.15
0.1
0.05
0
-0.05
-0.1
-0.15
$\log(D_V/D_K)$
−0.25
0
5
8
12
0.25
17
0.5
1.8
2
2.2
2.4
2.6
$\log(\sigma)$
1.8
1.6
1.4
1.2
1
0.8
0.6
0.4
$\log(D_K)$ (arcsec)
1.8
2
2.2
2.4
2.6
$\log(\sigma)$

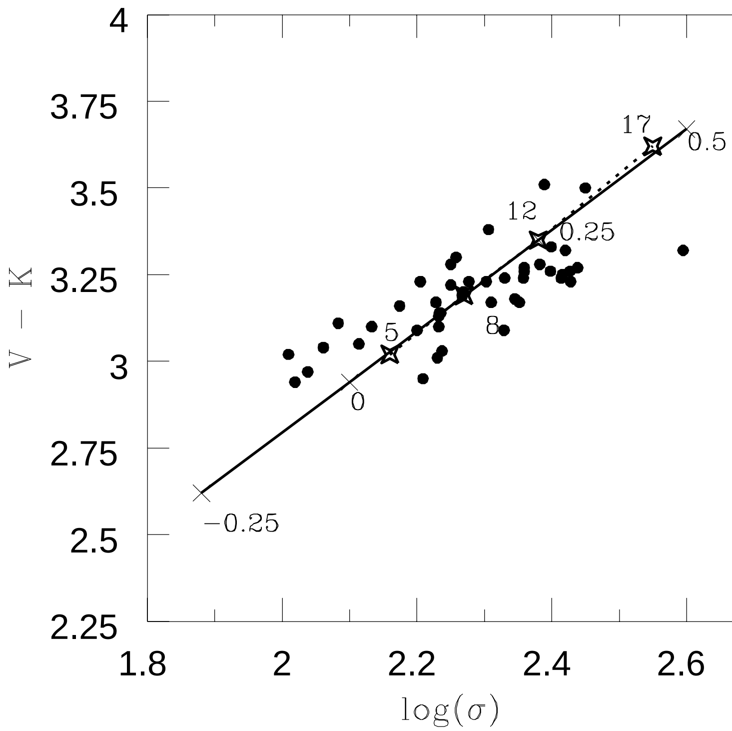

V − K
log(σ)
−0.25
0
5
8
12
0.25
17
0.5

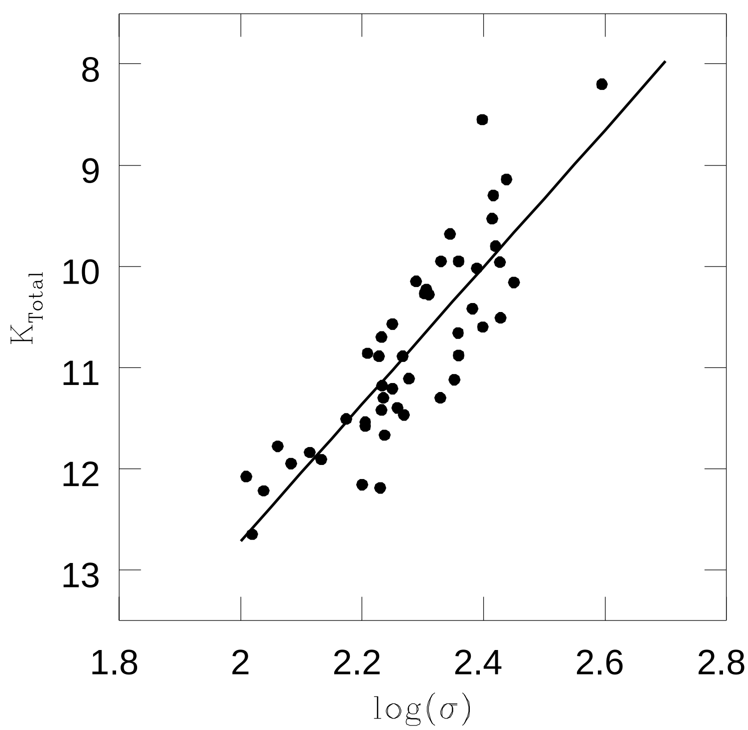

K_{Total}
log(σ)

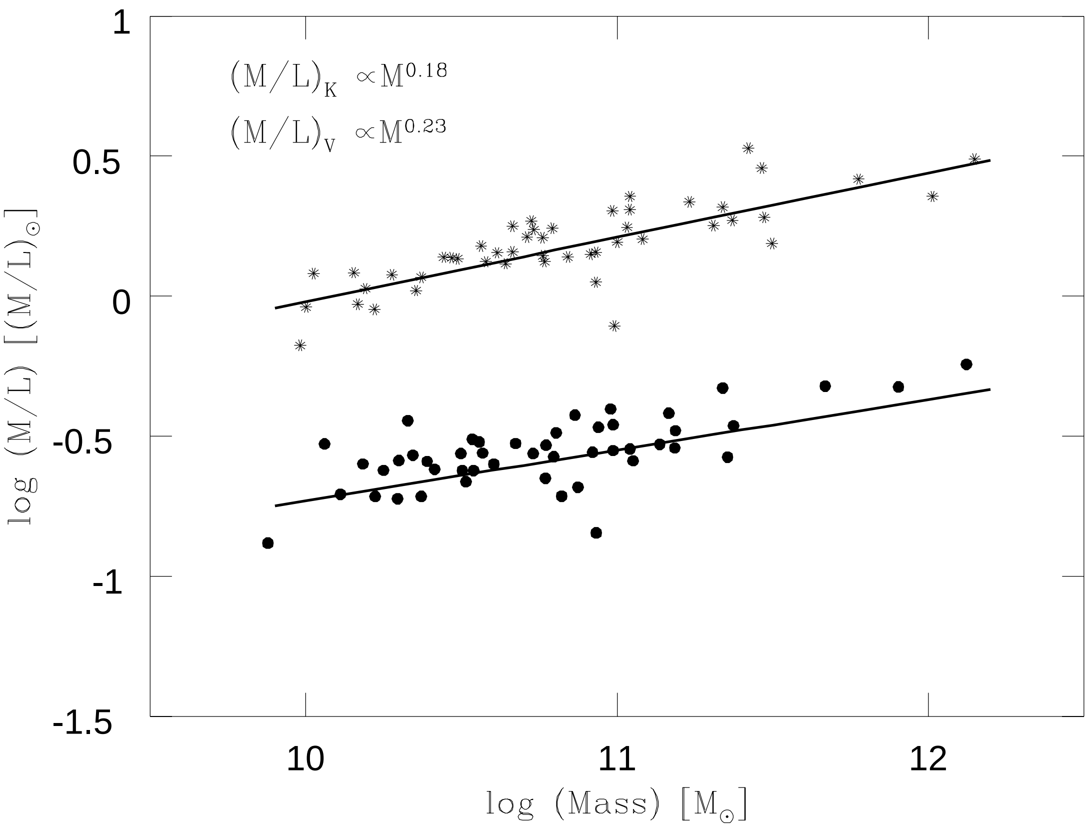

$(M/L)_K \propto M^{0.18}$
$(M/L)_V \propto M^{0.23}$
1
0.5
0
-0.5
-1
-1.5
log (M/L) [$(M/L)_\odot$]
10
11
12
log (Mass) [$M_\odot$]

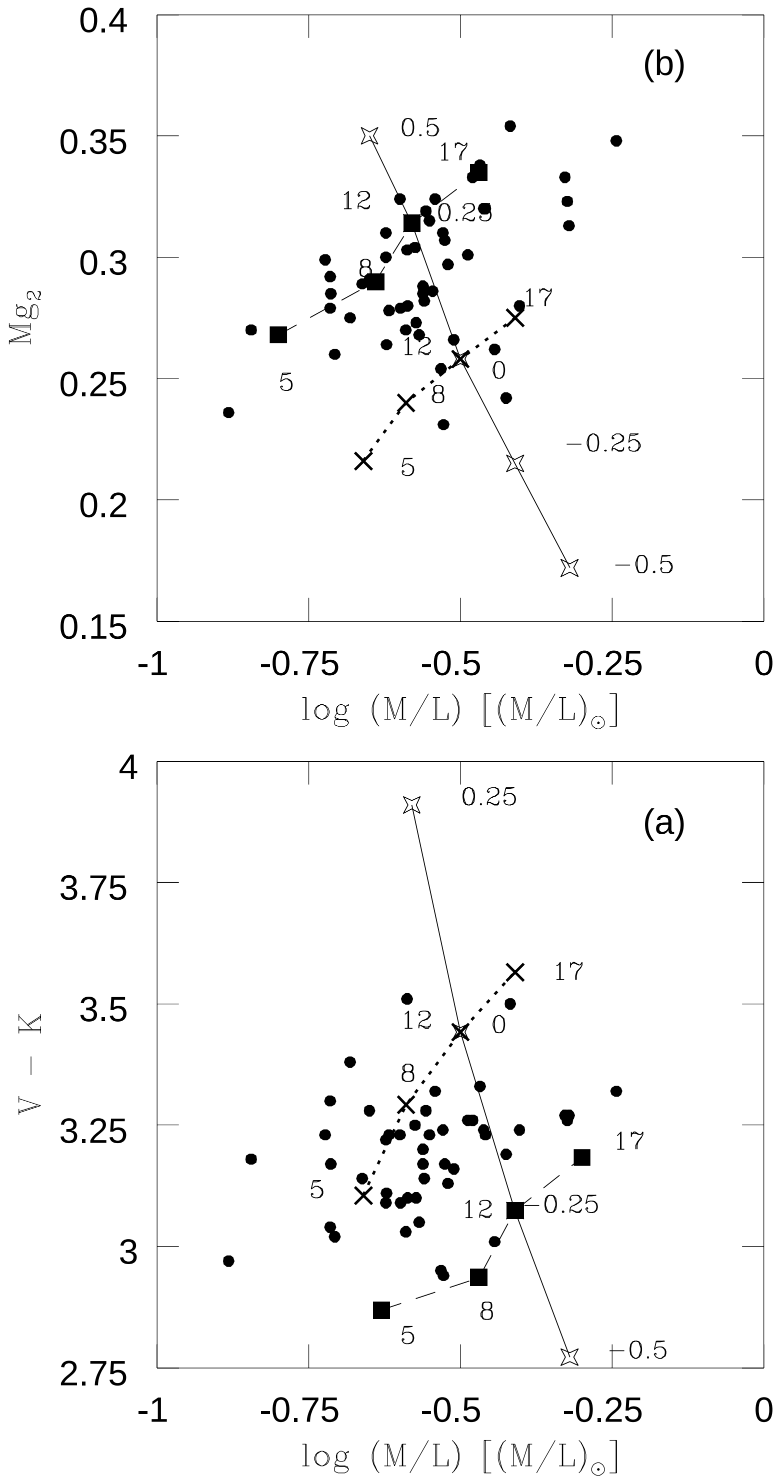

(b)
Mg$_2$
log (M/L) [(M/L)$_\odot$]
0.5
17
12
0.25
8
5
12
0
8
−0.25
5
−0.5
(a)
V − K
log (M/L) [(M/L)$_\odot$]
0.25
17
12
0
8
5
17
12
−0.25
8
5
−0.5